Title

Osteoblast-Specific Loss of IGF1R Signaling Results in Impaired Endochondral Bone Formation During Fracture Healing

Journal

Journal of Bone and Mineral Research, 30(9)

ISSN

0884-0431

Authors

Wang, Tao
Wang, Yongmei
Menendez, Alicia
et al.

Publication Date

2015-09-01

DOI

10.1002/jbmr.2510

Peer reviewed

HHS Public Access

Author manuscript

J Bone Miner Res. Author manuscript; available in PMC 2017 November 16.

Published in final edited form as:

J Bone Miner Res. 2015 September ; 30(9): 1572–1584. doi:10.1002/jbmr.2510.

Osteoblast-Specific Loss of IGF1R Signaling Results in Impaired Endochondral Bone Formation During Fracture Healing

Tao Wang[1,2], **Yongmei Wang**[1], **Alicia Menendez**[1], **Chak Fong**[1], **Muriel Babey**[1], **Candice GT Tahimic**[1], **Zhiqiang Cheng**[1], **Alfred Li**[1], **Wenhan Chang**[1], and **Daniel D. Bikle**[1]

[1]Endocrine Unit, VA Medical Center and University of California, San Francisco, CA, USA

[2]Department of Orthopedics, Civil Aviation General Hospital, Beijing, China

Abstract

Insulin-like growth factors (IGFs) are important local regulators during fracture healing. Although IGF1 deficiency is known to increase the risk of delayed union or non-union fractures in the elderly population, the underlying mechanisms that contribute to this defect remains unclear. In this study, IGF1 signaling during fracture healing was investigated in an osteoblast-specific IGF1 receptor (IGF1R) conditional knockout (KO) mouse model. A closed tibial fracture was induced in $IGF1R^{flox/flox}$/2.3-kb α1(1)-collagen-Cre (KO) and $IGF1R^{flox/flox}$ (control) mice aged 12 weeks. Fracture callus samples and nonfractured tibial diaphysis were collected and analyzed by μCT, histology, immunohistochemistry, histomorphometry, and gene expression analysis at 10, 15, 21, and 28 days after fracture. A smaller size callus, lower bone volume accompanied by a defect in mineralization, bone microarchitectural abnormalities, and a higher cartilage volume were observed in the callus of these KO mice. The levels of osteoblast differentiation markers (osteocalcin, alkaline phosphatase, collagen 1α1) were significantly reduced, but the early osteoblast transcription factor runx2, as well as chondrocyte differentiation markers (collagen 2α1 and collagen 10α1) were significantly increased in the KO callus. Moreover, increased numbers of osteoclasts and impaired angiogenesis were observed during the first 15 days of fracture repair, but decreased numbers of osteoclasts were found in the later stages of fracture repair in the KO mice. Although baseline nonfractured tibias of KO mice had decreased trabecular and cortical bone compared to control mice, subsequent studies with mice expressing the 2.3-kb α1(1)-collagen-Cre ERT2 construct and given tamoxifen at the time of fracture and so starting with comparable bone levels showed similar impairment in fracture repair at least initially. Our data indicate that not only is the IGF1R in osteoblasts involved in osteoblast differentiation during fracture repair, but it plays an important role in coordinating chondrocyte, osteoclast, and endothelial responses that all contribute to the endochondral bone formation required for normal fracture repair.

Address correspondence to: Tao Wang, MD, PhD, Endocrine Unit (111N), VAMC, University of California, San Francisco, 1700 Owens St, CA 94158, USA., taowang75@yahoo.com; daniel.bikle@ucsf.edu.

Disclosures

All authors state that they have no conflicts of interest.

Additional Supporting Information may be found in the online version of this article.

Keywords

IGF1 RECEPTOR; OSTEOBLASTS; FRACTURE HEALING; ENDOCHONDRAL BONE FORMATION; ANGIOGENESIS

Introduction

Insulin-like growth factor 1 (IGF1) is the most abundant growth factor stored in bone, and with its receptor IGF1R forms a major growth-promoting signaling system for the skeleton.[1] IGF1 plays many important roles in both bone development and remodeling. The growing skeleton is modulated by IGF1 through endocrine, paracrine, and autocrine mechanisms including its role in mediating the skeletal actions of growth hormone and PTH.[2] IGF1 exerts its action by binding to the IGF1R, which triggers a number of intracellular signaling pathways.[3]

A prospective clinical study showed that impairment of the growth hormone (GH)/IGF1 axis correlated to the quality of fracture healing, suggesting its involvement in the pathphysiological mechanisms determining delayed or failed fracture healing, and found that serum IGF1 concentrations of the non-union group were below those of the union group.[4] Members of the IGF family have been detected locally in the fracture callus of patients,[5] and these levels are increased during fracture healing in rats.[6] Circulating IGF1 is mainly produced in the liver stimulated by GH. Unlike classical peptide hormones, IGFs are widely expressed by cells with rapid rates of proliferation and in regenerating tissues such as osteoblasts, and function in a paracrine and autocrine manner in those tissues. Thus, circulating IGF1 has a role in bone remodeling, but endogenous, ie, skeletal, IGF1 production is likely to play the major role.[7]

The majority of fractures heal by the combination of both intramembranous and endochondral bone formation. The process includes cellular condensation, hypertrophic chondro-genesis, matrix mineralization, vascularization, bone formation, and callus remodeling through osteoclastic activity. During fracture healing, IGF1 is involved in cell proliferation and differentiation of mesenchymal cells, periosteal cells, osteoblasts, osteoclasts, and chondrocytes in an autocrine and/or paracrine fashion. There are numerous studies now showing evidence of communication between those cells, and a closed biological connection exists between these cells during fracture healing. IGF1 regulates osteoblastic proliferation, differentiation, survival, and the synthesis of bone matrix in vivo.[8–10] Osteoblasts also depend on IGF1 signaling to regulate osteoclastogenesis per se and as stimulated by PTH.[11,12] IGF1 stimulates VEGF secretion from both osteoblasts and chondrocytes to promote angiogenesis.[13] Moreover, osteoblasts and chondrocytes promote each other's differentiation process.[14] These data suggest that osteoblasts orchestrate interactions between different cell populations, playing a central role in fracture healing by coordinating the actions of the different cell types involved, and that most of those cell–cell communication functions are dependent on IGF1 signaling. However, the specific functions of IGF1 signaling in osteoblasts and their communication with other cells during fracture healing have not been previously determined. In this study, we hypothesized that disrupting

IGF1 signaling in osteoblasts would alter endochondral bone formation, mineralization, neovascularization, and callus remodeling during fracture healing. To test this hypothesis, we created an osteoblast-specific IGF1 signaling–deficient mouse model in which the *Igf1r* gene was ablated specifically in osteoblasts (OBIGF1R$^{-/-}$) by *Cre-lox* recombination. Our results demonstrated that deletion of the IGF1R from osteoblasts profoundly affected all aspects of fracture healing.

Materials and Methods

Generation of osteoblast-specific IGF1R knockout mice

The OBIGF1R$^{-/-}$(KO) mice were made by breeding *floxed-Igf1r* (*Igf1r*$^{flox/flox}$) mice that carry *loxP* sequences flanking exon 3 of the gene[15] with transgenic mice (*Cre*-*Col1*α1) expressing Cre recombinase under the control of a 2.3-kb Collagen1α1 [*Col1*α*1*] promoter[16] (Jackson Laboratories, Bar Harbor, ME, USA). We also generated tamoxifen-inducible, osteoblast-specific IGF1R knockout mice that permit osteoblast-specific knockout of *Igf1r* just prior to fracture. The inducible OBIGF1R$^{-/-}$ (iKO) mice were generated by breeding *Igf1r*$^{flox/flox}$ mice with mice expressing a *Cre ert2 2.3kbcol1a1* transgene, which encodes a fusion protein of the Cre recombinase and a mutated estrogen-responsive element to confer sensitivity to Tam.[17] Littermates not expressing the Cre recombinase served as controls. Gene disruption was induced by five i.p. injections of tamoxifen in oil (75 mg/kg body weight), and fracture was performed after the second Tam injection. Both experimental and control mice received the tamoxifen. All animal studies were done in accordance with and approval by the Animal Use Committee of the San Francisco Veterans Affairs Medical Center, where the animals were raised and studied.

Genotyping and determination of tissue-specific deletion of the IGF1R gene

Genomic DNA was extracted from tail snips and other tissues (spleen, muscle, lung, heart, gut, liver, growth plate cartilage, callas and bone) of the mice using DNeasy Blood and Tissue Kit (Qiagen, Valencia, CA, USA) for purification and Phire Animal Tissue Direct PCR Kit for amplification (Thermo Fisher Scientific Inc., Marietta, OH, USA). Polymerase chain reaction (PCR) analyses of the DNA were performed to detect Cre and floxed-IGF1R alleles using corresponding primer sets with standard conditions (5 min at 98°C; 5 s at 98°C, 5 s at 61°C, and 20 s at 72°C for 37 cycles; 1 min at 72°C; ∞ at 4°C). PCR was performed with a mixture of three primers (two forward primers, 5′-CTT CCC AGC TTG CTA CTC TAG G-3′ and 5′-TGA GAC GTA GCG AGA TTG CTG TA-3′, and a reverse primer, 5′-CAG GCTTGC AAT GAG ACA TGG G-3′) to detect 320-bp and 120-bp products from the non-excised and excised gene alleles, respectively.[18] The Cre transgene was detected by PCR using the primers 5′-GCA AAA CAG GCT CTA GCG TTC G-3′ (forward) and 5′-CTG TTT CAC TAT CCZ GGT TAC GG-3′ (reverse) to amplify a 560-bp DNA product. Cre-positive and gene excision (Δ-IGF1R) positive littermates were designated as experimental groups whereas Cre-negative littermates were used as controls.

Nonstabilized tibial fracture model and biomechanical testing

Twelve-week-old female KO mice, iKO mice, and their control littermates were anesthetized with isoflurane using a rodent gas anesthesia instrument. A Bose Electroforce 3200

mechanical instrument (Eden Prairie, Minnesota, USA) was used to create a closed tibial fracture model without fixation. Three-point bending was used to create the fracture in these mice, and both bending stiffness and strength were recorded at a rate of 0.05 mm/s. The fracture site occurred in the upper-middle portion of the right diaphysis and maximum load were evaluated for fractured legs. Mice received analgesics after fracture. The mice were allowed to recover on a heated pad, and, after awakening, they were returned to their cages and allowed to ambulate freely. Mice were sacrificed at 10, 15, 21, and 28 days after fracture. Calluses from the KO mice, iKO mice, and their control littermates were harvested for analysis.

μCT

All μCT measurements were carried out using a SCANCO MicroCT 50 scanner (SCANCO Medical AG, Bassersdorf, Switzerland). All scanning and evaluation was performed using a voxel size of 10 μm and slice increments of 10 μm. Quantitative analyses were carried out using the SCANCO Evaluation Program v6.0. Non-fractured control tibias (KO, iKO mice and their control mice, n =5 or 6 for each group, 12 weeks old) were evaluated at both the secondary spongiosa of the proximal metaphysis and at the cortical region where the fractures were made. For trabecular analysis in secondary spongiosa, we analyzed a region beginning at the growth plate and extending proximally for 100 slices. A lower threshold of 300 units, a Gaussian sigma of 0.5, and a Gaussian support of 2 were chosen as trabecular evaluation settings. For evaluation of cortical bone, a 40-slice region centered on the mid-diaphysis of the tibia was analyzed. This region was chosen to represent a similar anatomical location as the fracture sites in the contralateral tibias. A lower threshold of 380 units, a Gaussian sigma of 0.8, and a Gaussian support of 1 were chosen as cortical evaluation settings. For fracture callus analysis, we evaluated a 2-mm region of the callus centered on the site of fracture. Our analysis segregated newly formed bone by manually delineating a mask to exclude preexisting cortical bone. A thresholding algorithm protocol was used to segment mineralized tissue. Its settings are characterized by a lower threshold of 240 units, with a Gaussian sigma and support of 0.8 and 1, respectively. μCT imaging was performed at 10, 15, 21, and 28 days after fracture (n =5 or 6 per group). The following measures of bone and callus structure and composition were evaluated from the μCT data for each specimen: total volume (TV, mm^3), bone volume (BV, mm^3), bone volume fraction (BV/TV, %), trabecular thickness (Tb.Th, μm), trabecular number (Tb.N, 1/mm), and trabecular separation (Tb.Sp, μm), total cross-sectional area (Tt.Ar, mm^2), cortical bone area (Ct.Ar, mm^2), cortical area fraction (Ct.Ar/Tt.Ar, %), and cortical thickness (Ct.Th, μm).[19]

Bone histomorphometry

The mice were injected with calceindemeclocycline 4 days and 1 day prior to euthanasia. After μCT measurements, undecalcified tibias were embedded in methyl methacrylate (MMA). A microtome (RM 2265; Leica, Germany) was used to cut the embedded samples with sections taken through the entire callus tissue. Five-μm-thick plastic sections were stained with Goldner, von Kossa-safranin O/Fast Green, Toluidine blue, or tartrate-resistant acid phosphatase (TRAP) for visualization of osteoblasts and osteoclasts, respectively. The stained specimens were used for determining static and structural measurements while 10-μm-thick plastic sections was used for assessing dynamic measurements of bone formation.

The section stained by Von Kossa-safranin O/Fast Green, marking cartilage as red or pink and bone tissues as black, were used for the histomorphometric analyses of total callus and cartilage volumes. Three equidistant sections spaced at 250 μm apart throughout the midsagittal section of the callus were evaluated. Images of stained sections were captured using a Zeiss light microscope (Axio Imager 2; Carl Zeiss, Germany) with an attached high-resolution digital c-mount camera. Callus area was determined by selecting all pixels within the callus excluding the original cortical bone, bone marrow compartments, and soft tissues. The total area of the callus, cartilage, trabecular, and osteoid bone in mm^2 was determined by their stained color. Sections were analyzed semiautomatically using the Bioquant Osteo computerized image analysis system (R&M Biometrics, Nashville, TN, USA). Standard nomenclature was used to express the histomorphometric values: callus tissue area (T.Ar, mm^2), callus bone area (B.Ar, mm^2), callus bone volume (BV/TV, %), callus cartilage area (Cg.Ar, mm^2), callus cartilage volume (CV/TV, %), trabecular number (Tb.N, 1/mm), trabecular width (Tb.Wi, μm), trabecular separation (Tb.Sp, μm), callus osteoid volume/bone volume (OV/BV, %), osteoblast number (N.Ob/BS, 1/mm), osteoclast number (N.Oc/BS, 1/mm), mineralization lag time (Mlt, D), mineral apposition rate (MAR, μm/day), and bone formation rate (BFR/BS, $\mu m^3/\mu m^2$/day). [20] Those parameters were calculated by the Bioquant program. The mean of a set of data values was calculated from three sections per animal.

Immunohistochemistry

Callus samples were serially fixed in 10% normal buffered formaldehyde for 1 day, decalcified in 10% EDTA solution for 10 days, and then embedded in frozen blocks. Tissue sections at the fracture site were cut longitudinally by microtome at a thickness of 7 μm. Immunohistochemistry was performed using enzymatic Avidin-Biotin Complex–diaminobenzidine staining with hematoxylin used for counterstaining. Antibodies to IGF1R 1:200 (ab39398; Abcam) and CD31 1:50 (ab28364; Abcam) were used according to the manufacturer's instructions. Each immunostaining reaction was accompanied by a negative control, where the primary antibody was not included. Optical density per stained area (IOD/area) was used to quantify the CD31 expression by detecting in six different images taken at ×100 magnification from the location of the callus with Image Pro Plus 6.0 software (Media Cybernetics, MD, USA). Immunohistochemical staining was evaluated by computerized optical density (OD) measurements, which corresponded to the staining intensity. The standardization procedures for computer-assisted immunohistochemical staining quantification were described in detail elsewhere.[21] Briefly, positively stained regions of the image were selected by HSI (hue, saturation, and lightness) with S from 0 to 255, I from 0 to 210, and H from 0 to 25, and then the brown color was converted into grayscale signal. The grayscale CD31 signal was measured as mean optical intensity of staining (mean optical density [MOD]) within the tissue masks. For immunohistochemistry studies, at least four mice per group were examined. Three equidistant sections spaced at 250 μm apart throughout the midsagittal section of the callus were evaluated.

RNA levels in bone

RNA was isolated from fracture callus tissues at 10, 15, 21, and 28 days after fracture (n =4 or 5 at each time point). The callus of the fracture site was harvested and total RNA was

extracted and reverse transcribed into cDNA, as described.[22] Expression of osteocalcin (OCN), alkaline phosphatase (ALP), collagen type1, alpha 1 (Col1a1), runt-related transcription factor 2 (Runx2), collagen type 2, alpha 1 (Col2a1), collagen type 10, alpha 1 (Col10a1), receptor activator of NF-κB (RANK), receptor activator of NF κB ligand (RANKL), osteoprotegerin (OPG), and nuclear factor of activated T-cells cytoplasmic 1 (NFATc1) were determined by quantitative real-time PCR using specific murine primers and probes as described.[23,24] The ΔCt values were obtained by subtracting the L19 (as endogenous control) Ct values from the target gene Ct values of the same samples. The relative quantification of the target genes was calculated by the formula: $2^{-\Delta Ct}$.

Bone marrow stromal cell culture

Bone marrow stromal cells (BMSCs) were isolated from 12-week-old KO and their control littermates. Cells were cultured in 2 mL of modified essential medium (α-MEM) containing 10% fetal bovine serum (FBS) at a seeding density of 5×10^6 cells/well in 6-well plates. After 7 days in culture, the medium was replaced with medium containing 10 mM β-glycerophosphate and 50 mg/mL of ascorbic acid. This medium was changed every 2 days thereafter. On day 14 after plating, cells were harvested for mRNA isolation using the RNeasy Mini Kit (Qiagen, Valencia, CA, USA). After 14 days in culture, cells were also fixed and stained for alkaline phosphatase (ALP) positive colonies using a kit (Sigma Chemical, St. Louis, MO, USA). On day 21 after plating, cells were fixed for von Kossa staining to determine mineralization. The colonies greater than 2 mm^2 showing positive staining were quantified with Image Pro Plus 6.0 software.

Statistics

Based on literature and on our previous experience, for the μCT analysis of the bone volume fraction, with an SD of 8% and mean difference of 15% between the gene mutation group and control groups, 0.8 power will be achieved with a sample size of 5 for each group. Results were presented as mean ± SD and compared using the one-way ANOVA or unpaired Student's t test (Microsoft Excel 2010; Microsoft Corp., Redmond, WA, USA). All statistical tests were two-sided. Significance was assigned at $p < 0.05$.

Results

Gene excision and immunolocalization of IGF1R proteins

We confirmed the specificity of gene excision in the KO and iKO mice by PCR analyses of genomic DNA from different tissues with primers flanking exon 3 of the IGF1R gene and Cre transgene. As shown in Fig. 1*A*, *B*, the gene excision (Δ-IGF1R) and Cre transgene occurred in bone from the KO and iKO mice but not in other tissues from the same animals or in bone from the $IGF1R^{flox/flox}$ (control) mice, although a faint presumably nonspecific higher molecular weight band was seen in control liver tissue. The expression of IGF1R protein was profoundly reduced in osteoblasts in the woven bone of the callus in KO mice (Fig. 1*D*, *H*) compared to CON mice (Fig. 1*C*, *G*) and in iKO mice (Fig. 1*F*, *J*) compared to inducible control (iCON) mice (Fig. 1*E*, *I*).

Biomechanical testing analysis

Results of three-point bending testing showed that maximum load to create a tibial fracture was significantly decreased in KO mice compared to CON mice (p <0.05), whereas there were no significant differences in maximum load between iKO mice and their control mice (iCON) (Table 1).

μCT analysis of normal bone and callus

μCT data showed that both BV and BV/TV of the secondary spongiosa in the proximal tibial metaphysis were significantly decreased in baseline nonfractured KO mice compared to their control mice (Table 2). Cortical bone parameters, such as Ct.Ar, Ct.Ar/Tt.Ar, and Ct.Th at the targeted fracture site were also significantly decreased in the nonfractured KO mice (Table 2). μCT scout views taken at different times after fracture showed that the callus size in KO mice was smaller than that of CON mice. A clear fracture line can be seen in the callus of KO mice at 15 and 21 days indicating incomplete bony callus formation (Fig. 2). Both TV and BV at fracture sites were significantly decreased in KO mice compared to CON mice at early time points (day 10) and late time points (days 21 and 28) postfracture (p <0.05) (Fig. 3*A*, *B*). BV/TV, Tb.N, and Tb.Th at fracture sites were significantly decreased in KO mice at the last time point (day 28) (p <0.05) (Fig. 3*C*–*E*), and Tb.Sp was significantly increased in KO mice compared to CON mice at 10 days and 28 days postfracture (p <0.05) (Fig. 3*F*). These quantitative data demonstrated the delay in fracture healing in the KO mice.

No significant differences were found in the structural parameters of the spongiosa and cortical bone between nonfractured iKO and their CON genotypes, indicating that iKO and their CON mice were comparable prior to fracture (Supporting Table 1). However, TV and BV at the fracture site were significantly decreased in iKO mice compared to CON mice by day 10 postfracture (p <0.05) (Supporting Fig. 1A, B). Unlike the KO mice, the iKO appeared to recover by day 28 with an increase in BV (p <0.05) (Supporting Fig. 1B). We attribute this to the recovery of IGF1R in newly formed osteoblasts that are no longer exposed to tamoxifen.

Histomorphometric analyses of bone formation and mineralization

Histologic examination showed a reduction in new woven bone at 10, 21, and 28 days after fracture and increased cartilage within the callus at 10 and 15 days after fracture (Fig. 4). Quantification of the histomorphometric analyses is shown in Table 3. Both T.Ar and B.Ar were significantly decreased by days 10, 21, and 28 in the KO mice, compared to CON mice (p <0.05), and BV/TV, Tb.N, and Tb.Wi were significantly decreased in KO mice compared to CON mice at day 28 postfracture (p <0.05). Tb.Sp was significantly increased by days 10 and 28 in the KO mice (p <0.05). OV/BV was decreased at day 10 but increased by day 15, suggesting an initial delay in osteoblast formation followed by a delay in osteoblast function (mineralization). MAR and BFR/BS were significantly decreased by days 10 and 21 in the KO mice compared to CON mice (p <0.05), whereas Mlt was increased significantly in the KO at day 21 (p <0.05). Consistent with the μCT data, KO mice showed significantly smaller callus size, lower bone volume, and bone microarchitectural abnormalities that were accompanied by a defect in bone formation and mineralization during fracture healing.

These defects in bone formation and mineralization were accompanied by fewer osteoblasts over the surfaces of bone in the KO callus, relative to CON callus, with significant reductions on days 10, 21, and 28 (p <0.05) and near significance on day 15 (N.Ob/BS in Table 3).

Impaired osteoblastogenesis in the fracture of osteoblast-specific IGF1R knockout mice

We then examined markers of osteoblast differentiation in the fracture site. mRNA levels of OCN and ALP were significantly decreased on days 10 and 15 postfracture in the KO mice, and both ALP and Col1a1 were decreased on day 21 in the KO mice compared to CON mice (p <0.05) (Fig. 5*A*–*C*). On the other hand, Runx2 mRNA levels were significantly increased in the KO mouse fracture sites compared to that of CON mice at all time points (p <0.05) (Fig. 5*D*). Reduced osteoblast number despite the increase in Runx2 expression in the callus of KO mice indicated a block in osteoblast development at the osteoprogenitor stage in mice lacking IGF1R in their more mature osteoblasts.

Similar observations were made in iKO mice with decreased mRNA levels of OCN at 10, 15, and 21 days postfracture, decreased Col1a1 at 15 and 21 days postfracture, and increased Runx2 at 15 and 21 days postfracture compared to their control mice (p <0.05) (Supporting Fig. 2). On the other hand, these Col1a1 mRNA levels rebounded by day 28, consistent with the rebound in the BV of iKO mice noted earlier in μCT analysis of callus (Supporting Fig. 1B).

To determine whether mesenchymal stem cells from KO mice have impaired osteogenic potential, BMSCs flushed from KO and CON mice were isolated and placed in culture. Total RNA was extracted from the bone marrow cultures to examine the expression of genes associated with osteoblast differentiation. OBIGF1R$^{-/-}$ BMSC cultures had reduced expression of OCN and ALP (p <0.05) (Fig. 5*G*, *H*), compared to CON mice after 14 days in culture. This was associated with a reduction in alkaline phosphatase–positive and Von Kossa–positive colonies (Fig. 5*I*, *J*).

Delayed endochondral bone formation in the fracture of osteoblast-specific IGF1R knockout mice

As noted in Fig. 4, there was more cartilage scattered within the callus of the KO mice, and the cartilage volume (CV/TV, %) was increased quantitatively at days 10, 15, and 21 in the KO callus compared to CON callus. At day 28, the cartilage area was no longer detectable in either KO or CON mice (Table 3). Real-time PCR measurement confirmed these findings. Relative gene expression of Col2a1 and Col10a1, early and late markers of chondrocyte differentiation, respectively, showed that Col2a1 was significantly upregulated at all time points (p <0.05) (Fig. 5*E*), and Col10a1 was significantly increased at the day 15, 21, and 28 time points (p <0.05) (Fig. 5*F*). These findings indicated that there was a lag in endochondral bone formation in KO mice, which tended to have very high expression of the cartilage markers during the early stages (days 10 and 15) of fracture healing and stronger persistence of cartilage markers in the later stages (days 21 and 28) of fracture healing.

In iKO mice, CV/TV was increased at 10 days postfracture compared to their CON mice (p <0.05) (Supporting Fig. 3A). Likewise, the levels of Col2a1 were significantly increased in

the iKO compared to their CON mice at all time points, and Col10a1 was significantly increased at the 15-day and 21-day time points (p <0.05) (Supporting Fig. 3B, C). These data indicate that iKO results in the same delayed endochondral bone formation during fracture healing as the KO.

Biphasic effects of osteoclastogenesis in the KO mice

Osteoclastic activity is associated with both cartilage resorption and subsequent remodeling of the primary and secondary bone over the time course of fracture healing.[25] Significant increases in TRAP+ osteoclasts were observed in KO fracture sites, relative to CON, on day 15. However, at 21 and 28 days postfracture there was a decreased number of TRAP+ osteoclasts in KO calluses, compared to CON calluses (Fig. 6*A*–*P*). Quantitative analysis of the histomorphometric data showed that osteoclast number was significantly increased on day 15 but decreased on days 21 and 28 in the KO mice compared to CON mice (p <0.05) (N.Oc/BS in Table 3). We hypothesized that RANKL from the increased number of chondrocytes in the KO during the initial stages of fracture repair stimulated the increased number of osteoclasts, whereas a reduction in RANKL producing osteoblasts at later time points when high numbers of chondrocytes were no longer present would serve to reduce osteoclastogenesis. To test this hypothesis, we first measured expression of RANKL and OPG, two of the most prominent proteins involved in regulation of osteoclast formation.[26] The relative ratio of RANKL/OPG, an index of osteoclastogenesis, was increased at 15 days postfracture, but decreased by days 21 and 28 postfracture in KO mice compared to CON mice (p <0.05) (Fig. 6*Q*). NFATc1 and RANK expression was elevated, respectively, in the callus at days 10 and 15 in the KO mice, but both were reduced by days 21 and 28, compared with CON mice (p <0.05) (Fig. 6*Q*). These osteoclast-specific gene expression patterns were consistent with the observations of osteoclast numbers (N.Oc/BS) found in the KO calluses showing increased osteoclast numbers at the early time point (day 15) but decreased osteoclast numbers at later time points (day 21 and day 28).

Impaired angiogenesis in the callus of knockout mice

Angiogenesis and bone formation are coupled during skeletal development and fracture healing. The lack of oxygen (hypoxia) and the subsequent generation of angiogenic factors have been shown to be critical in achieving successful bone regeneration and fracture healing.[27] In order to assess vascular invasion of fracture calluses, CD31 immunohistochemical staining was used to quantify angiogenesis. CD31 is a transmembrane glycoprotein and is qualified as an endothelial cell marker. Microscopic image analysis showed that CD31 expression in KO callus was significantly decreased at the day 15 time point compared to CON mice (p <0.05) (Fig. 7*A*–*I*), paralleling a significant decrease in VEGF gene expression at this time point (p <0.05) (Fig. 7*J*). However, by day 21 this trend had reversed as VEGF expression increased.

Discussion

IGF1 plays a prominent regulatory role in skeletal development and bone remodeling. Deletion of *Igf1r* in osteoblasts impairs both the autocrine/paracrine and endocrine effects of IGF1 on osteoblasts. During the process of endochondral bone formation and fracture

healing, the immature osteoblast is essential for coupled vascular and osteogenic transformation.[28] Therefore, to reveal the role of IGF1 signaling in osteoblasts during fracture repair we used a transgenic mouse model expressing cre recombinase under control of a 2.3-kb collagen1α1 promoter, which enables specific expression in early differentiating osteoblasts.[29,30] In this animal model, no significant reductions in body size, femoral length, and tibial length by 12 weeks of age were found (data not shown), but there were significant reductions in proximal metaphyseal trabecular BV/TV (17.87%) and cortical bone parameters at the targeted fracture site, such as Ct.Ar (9.45%), Ct.Ar/Tt.Ar (8.37%), and Ct.Th (19.94%). Biomechanical tests showed reduced mechanical strength in the tibial diaphysis in these KO mice. Thus, deletion of *Igf1r* in osteoblasts using 2.3-kb Col1a1 promoter caused both trabecular and cortical bone loss and mechanically weaker cortical bone. For this reason we repeated the essence of our fracture experiments with a model in which IGF1R was deleted at the time of fracture with the same 2.3-kb col1a1 cre but under tamoxifen regulation. Because this construct does not delete genes (ie, *Igf1r)*) in stem cells, and we desired only a limited exposure to tamoxifen to avoid its skeletal effects, the iKO model likely provided only a transient deletion of *Igf1r*, sufficient, however, for comparisons to the KO model during the earlier time points postfracture.

Although the role of osteoblasts during fracture healing has been previously shown, the role of IGF1 signaling in osteoblasts during endochondral fracture repair had not been previously shown. Results from this study suggest that not only is IGF1 signaling in osteoblasts required for endochondral bone formation including the angiogenic response during fracture repair, but was also required for osteoclast activation in the later stages of fracture repair during remodeling of the bony callus. Blocking the IGF1-induced differentiation of osteoblasts at the stage of col1a1 expression resulted in a backlog of osteoprogenitors as indicated by the increase in Runx2 expression and decreased numbers of mature osteoblasts capable of bone formation during fracture repair. Moreover, although Runx2 directs multipotent mesenchymal cells toward an osteoblastic lineage, it maintains osteoblastic cells in an immature stage.[31] Overexpression of Runx2 inhibits osteoblast maturation and the transition of osteoblasts to osteocytes.[32,33] Therefore, in these KO mice, the overexpression of Runx2 due to disrupted IGF1 signaling may have contributed to the attenuation of osteoblast differentiation.

The increased cartilage volume, increased expression of markers of chondrocyte differentiation, and reduced bone in the KO and iKO mice suggest that the disruption of IGF1 signaling in osteoblasts also leads to a pileup of chondrocytes perhaps due to a defect in their terminal differentiation. Indeed it has been suggested that chondrocytes differentiate directly into osteoblasts, although our data do not speak to this point. The mechanism for the delayed conversion of cartilage to bone in KO and iKO mice is not understood at present, although it has been reported that there are interactions between chondrocytes and osteoblasts in co-culture that induce hypertrophic differentiation of the chondrocytes.[14] More recent studies have shown that EphB4, a member of the tyrosine kinase receptor Eph family, is expressed in osteoblasts as is its ligand ephrinB2, and both ephrin B2 and EphB4 are also expressed in late stage proliferating and prehypertrophic chondrocytes. The expression of ephrin B2 and EphB4 is stimulated by IGF1 and may provide a cell–cell communication mechanism between osteoblasts and chondrocytes to promote the transition

from cartilage to bone during endochondral bone formation.[34] This mechanism would be impaired in the OBIGF1R$^{-/-}$. However, the factors and interactions between osteoblasts and chondrocytes that contribute to fracture repair under the regulation of IGF1 signaling remain for future investigation.

The increase in osteoclasts during the initial stages of fracture repair but their decrease at later time points (day 21 and day 28) in the callus of KO mice was unexpected. However, chondrocytes produce RANKL, and their increased numbers during the early but not later stages of fracture repair in KO mice are consistent with the finding that the relative ratio of RANKL/OPG was increased at 15 days postfracture, but decreased by days 21 and 28 postfracture in KO mice compared to CON mice. The expression of RANKL and OPG plays an essential role in osteoclast recruitment during both the period of cartilage resorption and later during the remodeling of the primary and secondary bone over the time course of fracture healing.[35] It is also tempting to link these changes in the ratio of RANKL/OPG in KO mice to that of Runx2 expression, which was also quite elevated in the KO mouse callus on day 15 postfracture followed by a decrease at the 21-day and 28-day time points. Other studies have found that Runx2 overexpression in osteoblasts using the 2.3-kb Col1a1 promoter enhances osteoclastogenesis in vivo and ex vivo by upregulating RANKL, and reducing OPG expression.[33,36] The increased number of osteoclasts may have resulted in a reduced template for endochondral bone formation, which in turn interfered with the transition from cartilage to bone and impaired fracture healing.[37] However, with time the ratio of RANKL/OPG significantly decreased at 21-day and 28-day time points in KO mice. This is likely due to the reduction of osteoblasts in the callus of the KO mice compared to CON at a time of reduced chondrocytes as well, and the requirement for IGF1 signaling to promote RANKL expression in osteoblasts[34] and osteoblast-stimulated osteoclastogenesis.[11]

VEGF signaling plays a central role in neoangiogenesis and in endochondral bone formation. Osteoblasts and hypertrophic chondrocytes express VEGF, and have been implicated as primary regulators of angiogenesis in fracture healing.[38,39] IGF1, by activation of the PI3K pathway, induces VEGF expression in osteoblasts through transcriptional activation of hypoxia response genes.[40] CD31 immunohistochemistry and VEGF gene expression data showed decreased angiogenesis in the KO calluses at day 15. Oxygen is required for osteogenesis;[41] therefore, hypoxic conditions associated with decreased angiogenesis in the callus of KO mice may have contributed to the suppression of bone callous formation during the initial stages of fracture healing. However, angiogenesis recovered by day 21. Because VEGF mRNA expression by osteoblasts can be potently upregulated by hypoxia,[42] the initial hypoxia due to delayed angiogenesis appeared to be self correcting.

In conclusion, disrupting IGF1 signaling in the immature osteoblast significantly alters several phases of the fracture healing process. Our analyses indicate that there is a close link between osteoblasts and other cell populations involved with fracture healing, such as chondrocytes, osteoclasts, and vascular endothelial cells, which directly or indirectly is under the regulation of IGF1 signaling. Therefore, we believe that there is an increased risk of delayed unions and non-unions in patients with IGF1 signaling deficiency. However,

future studies are necessary to investigate the exact nature of the interactions between those cells contributing to fracture repair that are responsive to IGF1 signaling.

Supplementary Material

Refer to Web version on PubMed Central for supplementary material.

Acknowledgments

This work was supported by VA program project award IPIBX001599, NIH grant RO1AR055924, and NIH grant RO1DK054793. We thank Alfred Li for assistance with the three-point bending animal model and μCT analysis, and Zhiqiang Cheng and Fuqing Song for help with histology.

Authors' roles: Study design: TW, YW, and DB. Experimental conduct: TW, ZC, AL, WC, and MD. Data analysis: TW and DB. Animal work: AM and CF. Drafting manuscript: TW. Revising manuscript: TW, DB, and CT.

References

1. Trippel SB. Potential role of insulinlike growth factors in fracture healing. Clin Orthop Relat Res. 1998; 355(Suppl):S301–13.
2. Bikle DD, Sakata T, Leary C, et al. Insulin-like growth factor I is required for the anabolic actions of parathyroid hormone on mouse bone. J Bone Miner Res. 2002; 17(9):1570–8. [PubMed: 12211426]
3. Tahimic CG, Wang Y, Bikle DD. Anabolic effects of IGF-1 signaling on the skeleton. Front Endocrinol (Lausanne). 2013; 4:6. [PubMed: 23382729]
4. Weiss S, Henle P, Bidlingmaier M, et al. Systemic response of the GH/IGF-I axis in timely versus delayed fracture healing. Growth Horm IGF Res. 2008; 18(3):205–12. [PubMed: 17936052]
5. Andrew JG, Hoyland J, Freemont AJ, et al. Insulinlike growth factor gene expression in human fracture callus. Calcif Tissue Int. 1993; 53(2):97–102. [PubMed: 8402329]
6. Okazaki K, Jingushi S, Ikenoue T, et al. Expression of parathyroid hormone-related peptide and insulin-like growth factor I during rat fracture healing. J Orthop Res. 2003; 21(3):511–20. [PubMed: 12706025]
7. Zhao G, Monier-Faugere MC, Langub MC, et al. Targeted over-expression of insulin-like growth factor I to osteoblasts of transgenic mice: increased trabecular bone volume without increased osteoblast proliferation. Endocrinology. 2000; 141(7):2674–82. [PubMed: 10875273]
8. Bikle D, Majumdar S, Laib A, et al. The skeletal structure of insulin-like growth factor I-deficient mice. J Bone Miner Res. 2001; 16(12):2320–9. [PubMed: 11760848]
9. Nakae J, Kido Y, Accili D. Distinct and overlapping functions of insulin and IGF-I receptors. Endocr Rev. 2001; 22(6):818–35. [PubMed: 11739335]
10. Pfeilschifter J, Oechsner M, Naumann A, et al. Stimulation of bone matrix apposition in vitro by local growth factors: a comparison between insulin-like growth factor I, platelet-derived growth factor, and transforming growth factor beta. Endocrinology. 1990; 127(1):69–75. [PubMed: 2361486]
11. Wang Y, Nishida S, Elalieh HZ, et al. Role of IGF-I signaling in regulating osteoclastogenesis. J Bone Miner Res. 2006; 21(9):1350–8. [PubMed: 16939393]
12. Bikle DD, Wang Y. Insulin like growth factor-I: a critical mediator of the skeletal response to parathyroid hormone. Curr Mol Pharmacol. 2012; 5(2):135–42. [PubMed: 21787292]
13. Deckers MM, Karperien M, van der Bent C, et al. Expression of vascular endothelial growth factors and their receptors during osteoblast differentiation. Endocrinology. 2000; 141(5):1667–74. [PubMed: 10803575]
14. Nakaoka R, Hsiong SX, Mooney DJ. Regulation of chondrocyte differentiation level via co-culture with osteoblasts. Tissue Eng. 2006; 12(9):2425–33. [PubMed: 16995776]
15. Dietrich P, Dragatsis I, Xuan S, et al. Conditional mutagenesis in mice with heat shock promoter-driven cre transgenes. Mamm Genome. 2000; 11(3):196–205. [PubMed: 10723724]

16. Dacquin R, Starbuck M, Schinke T, et al. Mouse alpha1(I)-collagen promoter is the best known promoter to drive efficient Cre recombinase expression in osteoblast. Dev Dyn. 2002; 224(2):245–51. [PubMed: 12112477]
17. Metzger D, Li M, Chambon P. Targeted somatic mutagenesis in the mouse epidermis. Methods Mol Biol. 2005; 289:329–40. [PubMed: 15502196]
18. Zhang M, Xuan S, Bouxsein ML, et al. Osteoblast-specific knockout of the insulin-like growth factor (IGF) receptor gene reveals an essential role of IGF signaling in bone matrix mineralization. J Biol Chem. 2002; 277(46):44005–12. [PubMed: 12215457]
19. Bouxsein ML, Boyd SK, Christiansen BA, et al. Guidelines for assessment of bone microstructure in rodents using microcomputed tomography. J Bone Miner Res. 2010; 25(7):1468–86. [PubMed: 20533309]
20. Dempster DW, Compston JE, Drezner MK, et al. Standardized nomenclature, symbols, and units for bone histomorphometry: a 2012 update of the report of the ASBMR Histomorphometry Nomenclature Committee. J Bone Miner Res. 2013; 28(1):2–17. [PubMed: 23197339]
21. Iakovlev VV, Gabril M, Dubinski W, et al. Microvascular density as an independent predictor of clinical outcome in renal cell carcinoma: an automated image analysis study. Lab Invest. 2012; 92(1):46–56. [PubMed: 22042086]
22. Rodriguez L, Cheng Z, Chen TH, et al. Extracellular calcium and parathyroid hormone-related peptide signaling modulate the pace of growth plate chondrocyte differentiation. Endocrinology. 2005; 146(11):4597–608. [PubMed: 16099862]
23. Wang Y, Nishida S, Sakata T, et al. Insulin-like growth factor-I is essential for embryonic bone development. Endocrinology. 2006; 147(10):4753–61. [PubMed: 16857753]
24. Wallin J, Wilting J, Koseki H, et al. The role of Pax-1 in axial skeleton development. Development. 1994; 120(5):1109–21. [PubMed: 8026324]
25. Kon T, Cho TJ, Aizawa T, et al. Expression of osteoprotegerin, receptor activator of NF-kappaB ligand (osteoprotegerin ligand) and related proinflammatory cytokines during fracture healing. J Bone Miner Res. 2001; 16(6):1004–14. [PubMed: 11393777]
26. Yasuda H, Shima N, Nakagawa N, et al. Osteoclast differentiation factor is a ligand for osteoprotegerin/osteoclastogenesis-inhibitory factor and is identical to TRANCE/RANKL. Proc Natl Acad Sci U S A. 1998; 95(7):3597–602. [PubMed: 9520411]
27. Portal-Nunez S, Lozano D, Esbrit P. Role of angiogenesis on bone formation. Histol Histopathol. 2012; 27(5):559–66. [PubMed: 22419020]
28. Maes C, Kobayashi T, Selig MK, et al. Osteoblast precursors, but not mature osteoblasts, move into developing and fractured bones along with invading blood vessels. Dev Cell. 2010; 19(2):329–44. [PubMed: 20708594]
29. Kalajzic I, Kalajzic Z, Kaliterna M, et al. Use of type I collagen green fluorescent protein transgenes to identify subpopulations of cells at different stages of the osteoblast lineage. J Bone Miner Res. 2002; 17(1):15–25. [PubMed: 11771662]
30. Visnjic D, Kalajzic I, Gronowicz G, et al. Conditional ablation of the osteoblast lineage in Col2.3deltatk transgenic mice. J Bone Miner Res. 2001; 16(12):2222–31. [PubMed: 11760835]
31. Komori T. Regulation of osteoblast differentiation by transcription factors. J Cell Biochem. 2006; 99(5):1233–9. [PubMed: 16795049]
32. Liu W, Toyosawa S, Furuichi T, et al. Overexpression of Cbfa1 in osteoblasts inhibits osteoblast maturation and causes osteopenia with multiple fractures. J Cell Biol. 2001; 155(1):157–66. [PubMed: 11581292]
33. Geoffroy V, Kneissel M, Fournier B, et al. High bone resorption in adult aging transgenic mice overexpressing cbfa1/runx2 in cells of the osteoblastic lineage. Mol Cell Biol. 2002; 22(17):6222–33. [PubMed: 12167715]
34. Wang Y, Menendez A, Fong C, et al. Ephrin B2/EphB4 mediates the actions of IGF-I signaling in regulating endochondral bone formation. J Bone Miner Res. 2014; 29(8):1900–13. [PubMed: 24677183]
35. Gerstenfeld LC, Sacks DJ, Pelis M, et al. Comparison of effects of the bisphosphonate alendronate versus the RANKL inhibitor denosumab on murine fracture healing. J Bone Miner Res. 2009; 24(2):196–208. [PubMed: 19016594]

36. Enomoto H, Shiojiri S, Hoshi K, et al. Induction of osteoclast differentiation by Runx2 through receptor activator of nuclear factor-kappa B ligand (RANKL) and osteoprotegerin regulation and partial rescue of osteoclastogenesis in Runx2$^{-/-}$ mice by RANKL transgene. J Biol Chem. 2003; 278(26):23971–7. [PubMed: 12697767]

37. Kayal RA, Tsatsas D, Bauer MA, et al. Diminished bone formation during diabetic fracture healing is related to the premature resorption of cartilage associated with increased osteoclast activity. J Bone Miner Res. 2007; 22(4):560–8. [PubMed: 17243865]

38. Ai-Aql ZS, Alagl AS, Graves DT, et al. Molecular mechanisms controlling bone formation during fracture healing and distraction osteogenesis. J Dent Res. 2008; 87(2):107–18. [PubMed: 18218835]

39. Gerber HP, Vu TH, Ryan AM, et al. VEGF couples hypertrophic cartilage remodeling, ossification and angiogenesis during endochondral bone formation. Nat Med. 1999; 5(6):623–8. [PubMed: 10371499]

40. Akeno N, Robins J, Zhang M, et al. Induction of vascular endothelial growth factor by IGF-I in osteoblast-like cells is mediated by the PI3K signaling pathway through the hypoxia-inducible factor-2alpha. Endocrinology. 2002; 143(2):420–5. [PubMed: 11796494]

41. Utting JC, Robins SP, Brandao-Burch A, et al. Hypoxia inhibits the growth, differentiation and bone-forming capacity of rat osteoblasts. Exp Cell Res. 2006; 312(10):1693–702. [PubMed: 16529738]

42. Steinbrech DS, Mehrara BJ, Saadeh PB, et al. VEGF expression in an osteoblast-like cell line is regulated by a hypoxia response mechanism. Am J Physiol Cell Physiol. 2000; 278(4):C853–60. [PubMed: 10751333]

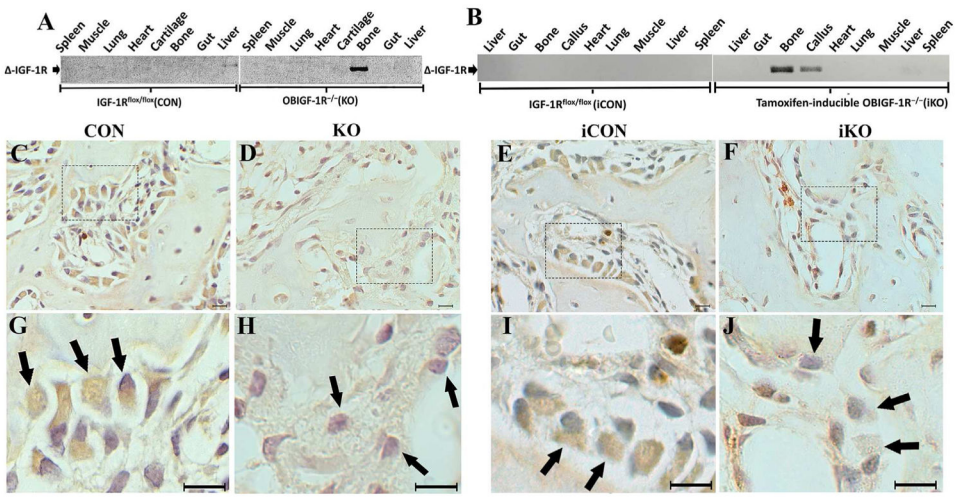

Fig. 1.

Specificity of the ablation of the *Igf1r* gene in osteoblasts. (*A*, *B*) PCR analyses of genomic DNA extracted from different tissues as specified from the KO and iKO mice and their control littermates with *Igf1r* gene excision (Δ-IGF-1R). (*C*–*F*) Immunohistochemistry for the expression of IGF1R in the osteoblasts (arrows) along the woven bone surface in the callus of KO and iKO mice and their control littermates (10 days after fracture). Bars =10 μm. (*G*–*J*) These observations are further confirmed by higher magnification. Bars =10 μm.

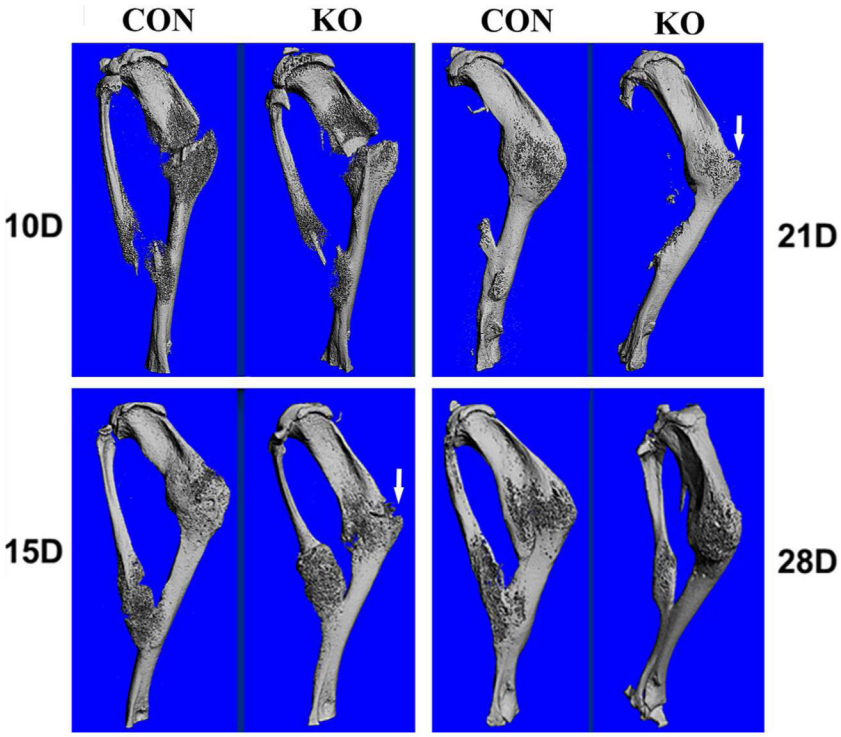

Fig. 2.

μCT scout view of fracture healing in KO and CON mice. After closed tibial fracture the time-course imaging of the callus showed that KO mice had a smaller size of callus and a residual fracture line (arrow) within the callus even after 21 days.

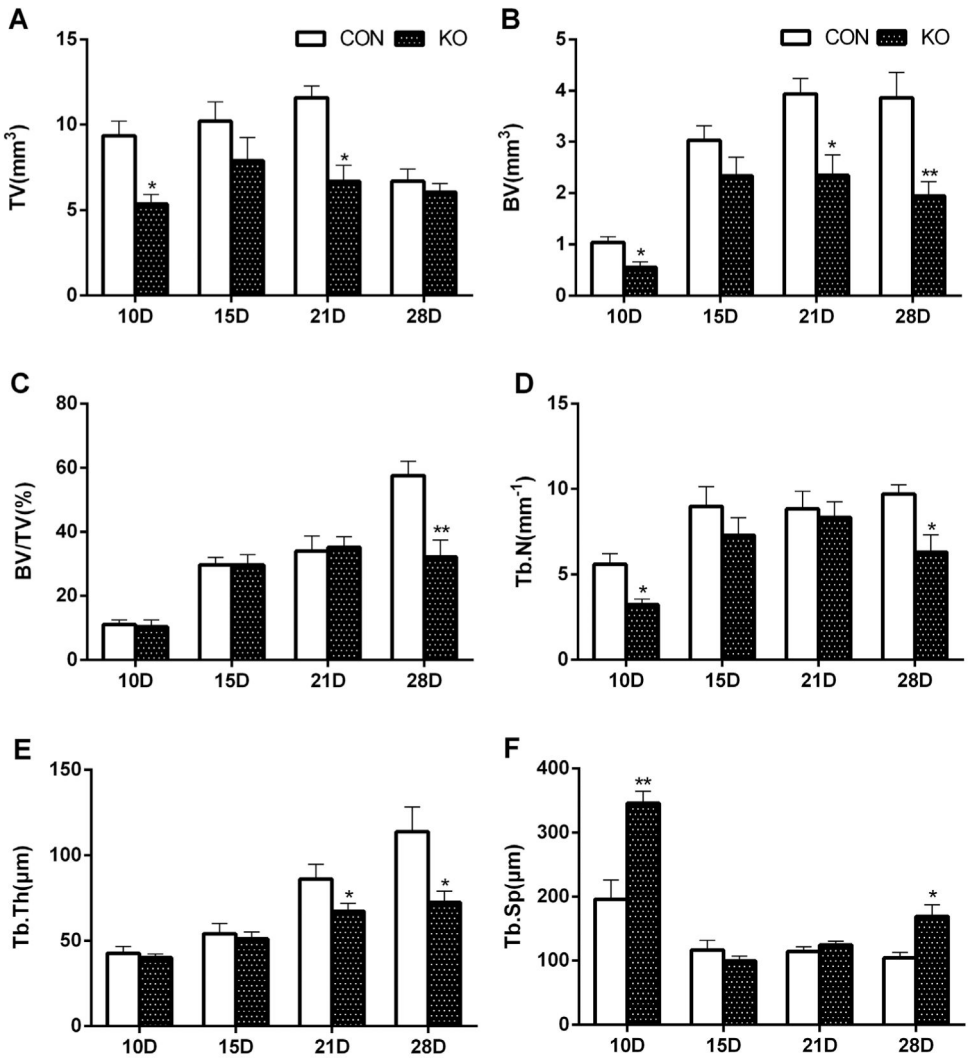

Fig. 3.

Disruption of IGF1 signaling in osteoblasts impairs osteogenesis and fracture healing in KO mice. μCT data showed that KO mice had a reduction in TV (Fig. 3*A*), BV (Fig. 3*B*), Tb.N (Fig. 3*D*) and Tb.Th (Fig. 3*E*) in the callus, although BV/TV ((Fig. 3*C*) was not significantly reduced until 28 days postfracture. Tb.Sp was significantly increased in KO mice compared to CON mice at 10 days and 28 days postfracture (Fig. 3*F*) (n =5 or 6 per group at each time point). *p <0.05; **p <0.01 versus control at the same time point. Data are expressed as mean ± SD.

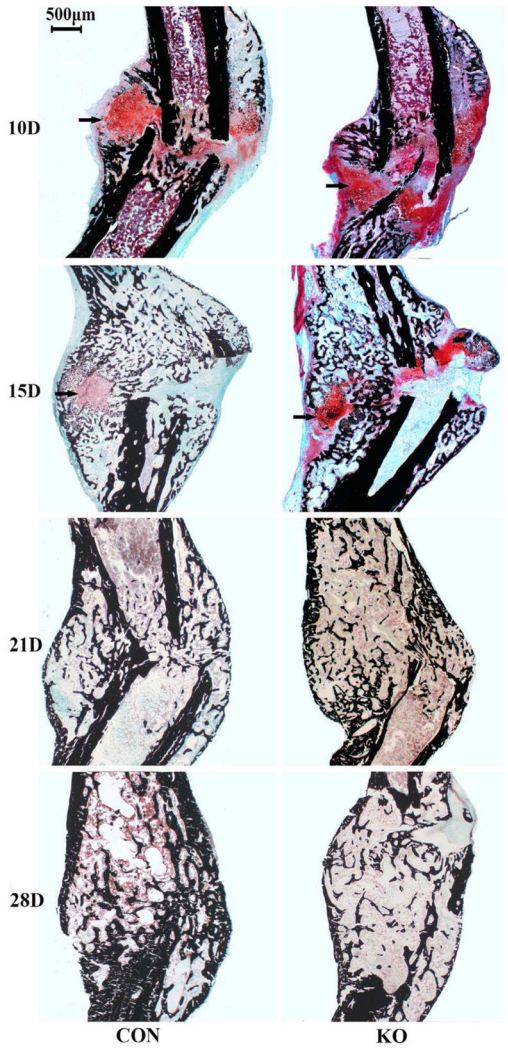

Fig. 4.

Histological analysis of fracture healing in KO and CON mice. von Kossa-safranin O/Fast green staining was used to stain bone black and cartilage red (arrow) in undecalcified sections of tibial fractures. A reduction in new woven bone at 10, 21, and 28 days after fracture and increased cartilage within the callus at 10 and 15 days after fracture are found in the callus of KO mice compared to CON mice. Bar =500 μm (n =5 per group at each time point).

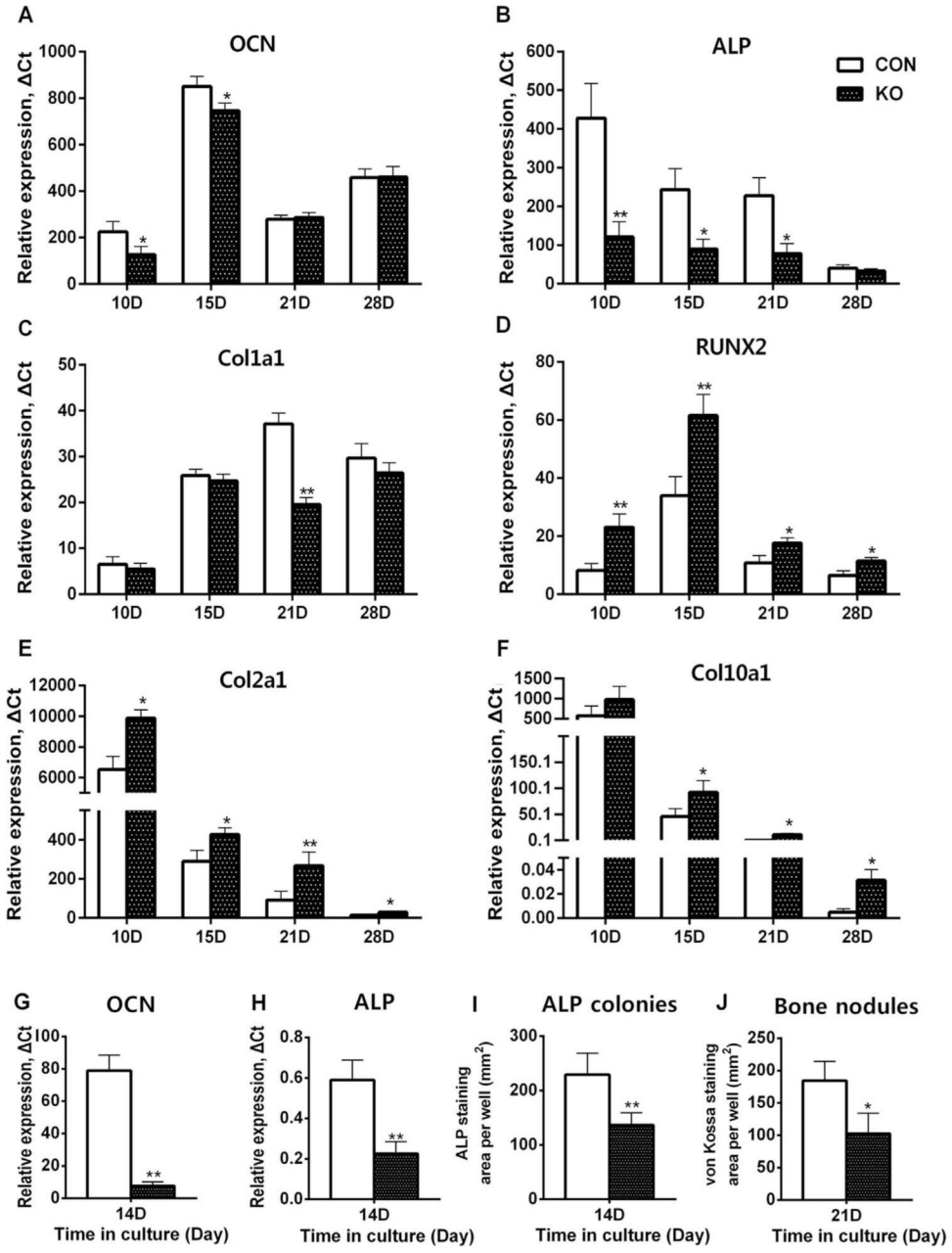

Fig. 5.

Gene analysis of fracture healing and bone marrow cultures. Gene expression levels of (*A*) OCN, (*B*) ALP, (*C*) Col1a1, (*D*) Runx2, (*E*) Col2a1, and (*F*) Col10a1 in tibia fracture calluses. Gene expression levels of (*G*) OCN, (*H*) ALP, and the osteoblast differentiation and mineralization indicators of (*I*) ALP colonies and (*J*) bone nodules in bone marrow stromal cell culture. n =4 or 5 per group at each time point. The mRNA levels were normalized to those of L_{19}. Cultures were assayed in triplicate wells. *$p < 0.05$, **$p < 0.01$ versus control at the same time point. Mean ± SD is shown.

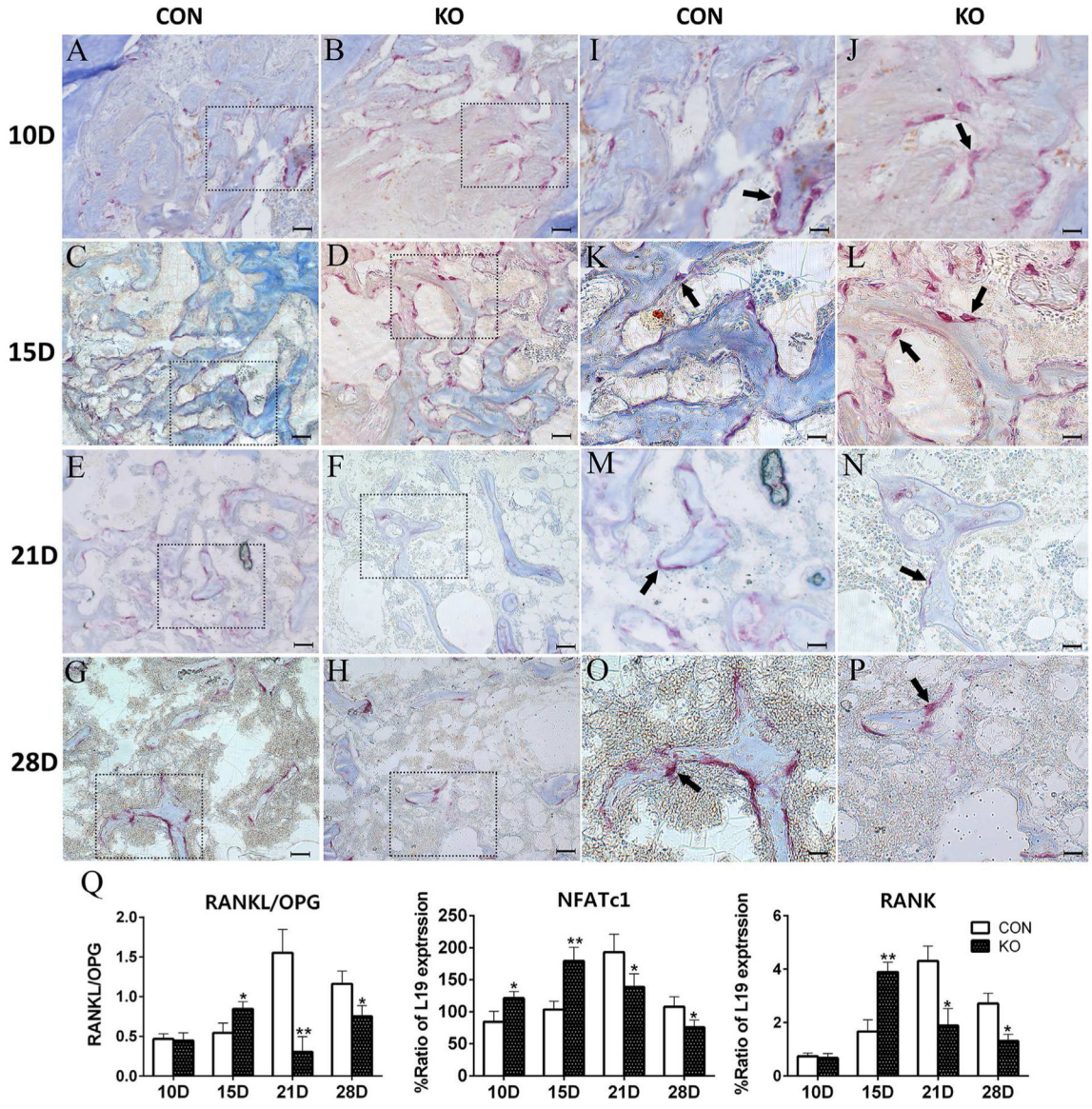

Fig. 6.

Deletion of Igf1r in osteoblasts induces a biphasic effect on osteoclastogenesis. (*A–H*) TRAP staining was performed on undecalcified sections of fractured tibia, and representative photomicrographs are shown at × 200 original magnification. Osteoclast numbers (arrows) were counted in 3 sections per mouse. Bars =200 μm. (*I–P*) These observations are further confirmed by higher magnification. Bars =20 μm. (n =4 or 5 per group at each time point). (*Q*) RANKL/OPG, NFAc1, and RANK RNA levels in the fracture callus were determined by RT-PCR (n =4 or 5 per group at each time point). *p <0.05, **p <0.01 versus control at the same time point. Mean ± SD is shown.

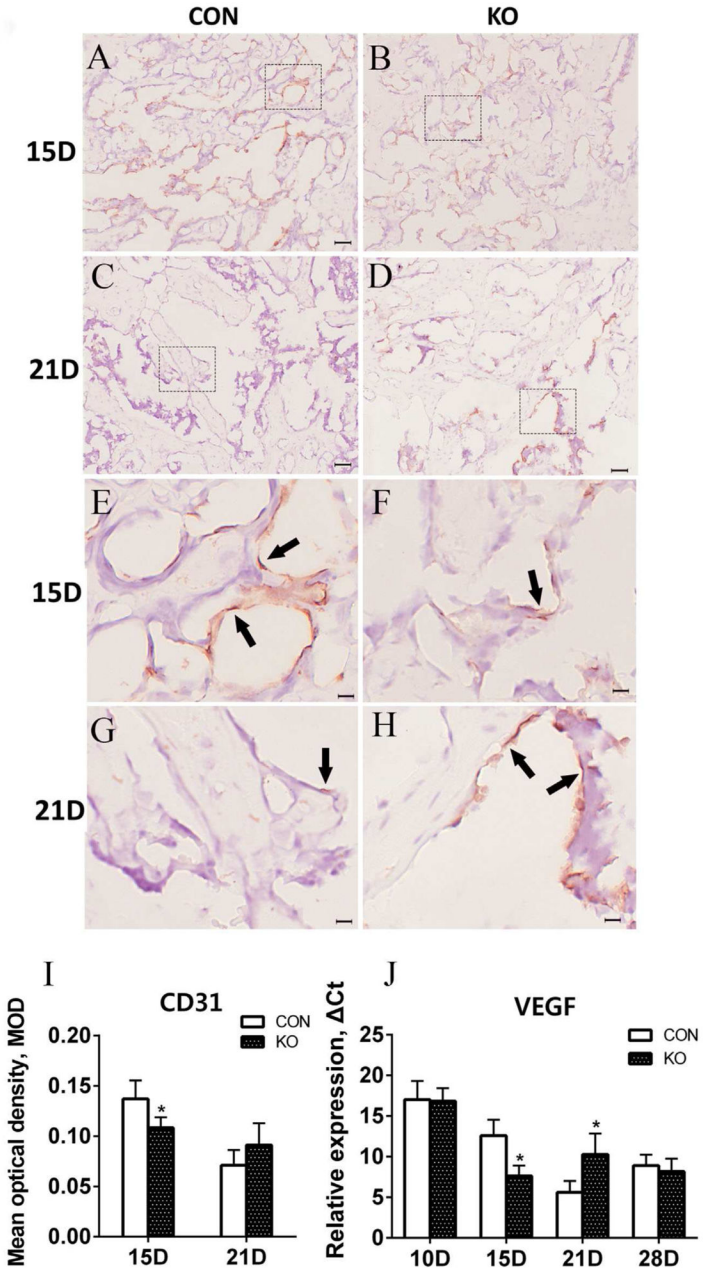

Fig. 7.

Deletion of Igf1r in osteoblasts impairs angiogenesis during the initial phase of fracture healing. (*A–D*). Immunohistochemistry for the expression of CD31 in the woven bone of callus. A representative section is shown. Bars =200 μm (n =4 or 5per group at each time point). Magnification: × 200. (*E–H*) The CD31 signal of brown DAB staining (arrows in higher magnification of the black-framed area) in the fracture callus was evaluated using computerized optical density (OD) measurements by Image Pro Plus in decalcified sections of fractured tibia. Bars =20μm. (*I*) The grayscale CD31 signal was measured as mean optical intensity of staining (mean optical density [MOD]) within the tissue masks. (*J*) The levels of

VEGF in the fracture callus were examined by RT-PCR (n =4 or 5 per group at each time point). *p <0.05 versus control at the same time. Mean ± SD is shown.

Table 1

Three-Point Bending Test

Group	Maximum load (N)
CON	27.83 ± 3.34
KO	22.52 ± 2.36 *
iCON	28.64 ± 3.10
iKO	27.46 ± 2.04

Values are shown as mean ± SD; n =10 per group at 12 weeks.

CON =control; KO =knockout; iCON =inducible control; iKO =inducible knockout.

* p <0.05 versus CON group.

Table 2

µCT Determination of the Structure of the Proximal Tibia and Cortical Bone at Fracture Site

Trabecular parameters	**TV (mm^3)**	**BV (mm^3)**	**BV/TV (%)**	**TB.Th (µm)**
CON	1.72 ± 0.06	0.22 ± 0.04	12.93 ± 1.26	40.70 ± 4.62
KO	1.62 ± 0.10	0.16 ± 0.04 *	10.62 ± 1.34 *	35.31 ± 6.33
Cortical parameters	Tt.Ar (mm^2)	Ct.Ar (mm^2)	Ct.Ar/Tt.Ar (%)	Ct.Th (µm)
CON	1.19 ± 0.11	0.74 ± 0.05	61.86 ± 1.87	191.53 ± 19.09
KO	1.19 ± 0.08	0.67 ± 0.05 *	56.68 ± 1.70 *	153.33 ± 7.08 *

Values are shown as mean ± SD; $n = 6$ per group at 12 weeks.

CON =control; KO =knockout.

* $p < 0.05$ versus control.

Table 3

Bone and Cartilage Histomorphometry

	10 days		15 days		21 days		28 days	
Bone parameters	**CON**	**KO**	**CON**	**KO**	**CON**	**KO**	**CON**	**KO**
Bone structure and bone formation								
Callus tissue area (T.Ar, mm^2)	4.82 ± 0.65	4.03 ± 0.55	6.53 ± 0.57	6.36 ± 0.64	5.77 ± 0.59	4.73 ± 0.43*	7.58 ± 0.71	6.52 ± 0.54*
Callus bone area (B.Ar, mm^2)	0.86 ± 0.11	0.78 ± 0.13	1.26 ± 0.14	1.18 ± 0.10	1.81 ± 0.12	1.31 ± 0.02*	2.67 ± 0.29	1.27 ± 0.37*
Callus bone volume (BV/TV, %)	21.13 ± 3.44	19.28 ± 2.13	19.32 ± 2.37	18.56 ± 3.28	31.37 ± 3.69	29.59 ± 2.26	35.16 ± 4.45	19.47 ± 4.36*
Trabecular number (Tb.N, 1/mm)	8.36 ± 1.62	7.63 ± 1.83	9.23 ± 1.16	8.16 ± 1.03	7.69 ± 1.02	8.91 ± 0.91	7.52 ± 1.56	6.30 ± 0.65*
Trabecular width (Tb.Wi, μm)	23.06 ± 3.80	24.10 ± 2.14	16.36 ± 4.05	19.63 ± 3.02	40.80 ± 7.67	32.23 ± 5.6	62.35 ± 8.46	37.15 ± 5.67*
Trabecular separation (Tb.Sp, μm)	87.97 ± 10.3	100.89 ± 8.4	72.26 ± 8.23	84.36± 6.56	84.25 ± 6.35	80.04 ± 7.15	71.89 ± 9.63	94.03 ± 11.20*
Osteoblast number (N.Ob/BS, 1/mm)	36.82 ± 6.21	18.43 ± 2.36*	46.89 ± 5.36	36.87 ± 4.65	39.33 ± 3.6	24.54 ± 4.12*	36.05 ± 5.56	26.36 ± 2.36*
Callus osteoid volume/bone volume (OV/BV, %)	8.12 ± 1.43	2.36 ± 0.86*	15.79 ± 1.62	19.52 ± 2.12*	13.23 ± 1.96	9.56 ± 1.64	3.13 ± 0.79	3.22 ± 1.04
Bone erosion								
Osteoclast number (N.Oc/BS, 1/mm)	2.36 ± 0.89	3.95 ± 0.93	5.06 ± 1.13	10.17 ± 1.62**	8.12 ± 1.53	3.20 ± 1.37*	9.20 ± 1.63	4.90 ± 0.94*
Bone dynamics								
Mineral apposition rate (MAR, mm/day)	2.50 ± 0.53	1.29 ± 0.49*	3.45 ± 0.34	3.30 ± 0.53	3.81 ± 0.48	2.10 ± 0.36*	2.70 ± 0.52	2.57 ± 0.37
Bone formation rate (BFR/BS, $\mu m^3/\mu m^2$/day)	0.96 ± 0.24	0.56 ± 0.17*	1.68 ± 0.12	1.45 ± 0.207	2.82 ± 0.32	1.48 ± 0.63*	1.70 ± 0.35	1.12 ± 0.27
Mineralization lag time (Mlt, D)	0.77 ± 0.09	0.97 ± 0.13	2.65 ± 0.47	3.54 ± 0.71	1.26 ± 0.23	3.72 ± 0.73*	1.03 ± 0.10	1.20 ± 0.54
Cartilage parameters								
Callus cartilage volume (CV/TV, %)	12.41 ± 2.4	27.77 ± 2.63**	3.58 ± 1.36	8.52 ± 1.693*	0.52 ± 0.21	1.32 ± 0.43*	0	0

Values are shown as mean ± SD; n =5 per group.

CON =control; KO =knockout.

* p <0.05 versus control at the same time point.

** p <0.01 versus control at the same time point.